Efficient and Accurate Bulk Parameterizations of Air–Sea Fluxes for Use in General Circulation Models

A. BIROL KARA

Sverdrup Technology Incorporated, Stennis Space Center, Mississippi

PETER A. ROCHFORD AND HARLEY E. HURLBURT

Naval Research Laboratory, Stennis Space Center, Mississippi

(Manuscript received 16 July 1999, in final form 20 December 1999)

ABSTRACT

Efficient and computationally inexpensive simple bulk formulas that include the effects of dynamic stability are developed to provide wind stress, and latent and sensible heat fluxes at the air–sea interface in general circulation models (GCMs). In these formulas the exchange coefficients for momentum and heat (i.e., wind stress drag coefficient, and latent and sensible heat flux coefficients, respectively) have a simple polynomial dependence on wind speed and a linear dependence on the air–sea temperature difference that are derived from a statistical analysis of global monthly climatologies according to wind speed and air–sea temperature difference intervals. Using surface meteorological observations from a central Arabian Sea mooring, these formulas are shown to yield air–sea fluxes on daily timescales that are highly accurate relative to those obtained with the standard algorithm used by the Tropical Ocean Global Atmosphere Coupled Ocean–Atmosphere Response Experiment (TOGA COARE), where the latter includes the effect of dynamic stability in calculating wind stress and air–sea heat fluxes. Direct comparisons in calculating the wind stress, and latent and sensible heat fluxes with these formulas and the TOGA COARE algorithm demonstrate that the methodology presented here is computationally inexpensive because iterative calculations are not required in the present methodology. Wind stress and air–sea fluxes can be calculated ≈30 times faster with these bulk formulas than by using the TOGA COARE algorithm. This methodology is of direct practical value for GCMs of high spatial resolution, where the severe computational demands of performing GCM simulations encourage computing air–sea fluxes in the most computationally efficient manner possible. The combination of accuracy and ease of computation of this method makes it the preferred one for computing air–sea fluxes in such GCMs.

1. Introduction and motivation

Momentum and heat fluxes at the air–sea interface constitute the principal coupling between the ocean and atmosphere, and are important quantities in governing the exchange of energy between these two systems. In ocean general circulation models (OGCMs), the wind stress is a major driving force for basin-scale upper-ocean circulation (e.g., Chen et al. 1994; Shriver and Hurlburt 1997), and the heat fluxes are important for determining the thermal properties of the upper ocean (e.g., Yuen et al. 1992; Swenson and Hansen 1999). Therefore, both heat and momentum fluxes are important for the development of sea surface temperature (SST), because of their contribution to turbulent mixing within the ocean surface mixed layer (e.g., Barnier 1998).

In an atmosphere GCM (AGCM) (e.g., Hogan and Rosmond 1991), the heat flux forcing experienced by the latter's lower boundary is required in the prognostic equation for surface air temperature. The latter is in turn required to compute vertical fluxes throughout the atmospheric planetary boundary layer (Stull 1988). In atmospheric models where the surface air temperature or SST is obtained from a surface energy balance, calculation of the latent and sensible heat fluxes becomes a critical issue for airmass transformation (Kara et al. 1998). It is thus no surprise that good representation of air–sea fluxes is important when performing large-scale GCM simulations of the atmosphere and ocean (e.g., Atlas 1987; Atlas et al. 1987; Price et al. 1987), and that good knowledge of the air–sea fluxes enhances the predictive skill of atmosphere, ocean, and coupled ocean–atmosphere GCMs.

In GCM simulations, flux forcing is typically applied in one of three ways: 1) using prescribed fields that are obtained from a variety of sources [e.g., climatology (da Silva et al. 1994), GCMs (Kallberg 1998), satellite and

Corresponding author address: Peter A. Rochford, Naval Research Laboratory, Bldg. 1009, Stennis Space Center, MS 39529.
E-mail: rochford@nrlssc.navy.mil

buoy observations for SST (Cummings et al. 1997)]; 2) fluxes determined using bulk parameterizations that only depend on properties across the air–sea interface [e.g., for latent and sensible heat fluxes (Hogan and Rosmond 1991)]; and 3) fluxes computed using turbulence-based formulations (e.g., Fairall et al. 1996). The first method is solely used for atmosphere (ocean) only GCM simulations, where a gridded in space and time SST (wind stress, heat flux) field is interpolated to the model grid at each time step. The second and third methods are used in an AGCM (OGCM), where the required ocean (atmosphere) properties are provided by a prescribed field, or some other means, such as an advective mixed layer (Murtugudde et al. 1996). In an OGCM (AGCM), the heat flux forcing is sometimes in the form of a relaxation of SST (surface air temperature) to a satellite-derived or climatology field (Chu et al. 1998) and is essentially a flux correction for the model. Flux corrections of this and other forms are commonly used in a coupled GCM to prevent climate drift (Sausen et al. 1988). They are implemented out of necessity to compensate for the inability of a coupled GCM to correctly simulate the thermal structure associated with the major ocean currents (Roberts et al. 1997). The magnitude of these flux adjustments diminishes considerably when regions of high horizontal SST gradient are carefully treated in air–sea flux calculations.

One advantage in using prescribed fields is the assurance of accurate forcing for the AGCM or OGCM. A second advantage is it is the most computationally inexpensive of the three methods for determining air–sea fluxes. The disadvantage is the use of prescribed fields precludes the possibility of any feedback mechanisms between the atmosphere and ocean. The latter becomes an important limitation if one is developing an AGCM or OGCM for implemententation as a component of a coupled GCM. For a coupled GCM, use of prescribed fields defeats the intent of the model, which is to fully simulate the physical interaction between the atmosphere and ocean, including its energy exchange. This limitation motivates the use of bulk formulas and turbulence models to determine the air–sea fluxes, as the response of the ocean (atmosphere) to atmospheric (oceanic) events can be incorporated into the flux calculation at every time step of the GCM simulation. For example, using the model SST in the surface fluxes of an OGCM simulation automatically provides a physically realistic tendency toward the ''correct'' SST, which is sufficient to keep the model SST on track (McCreary et al. 1993).

Bulk formulas are empirical equations that seek to represent, in a simple form, the air–sea fluxes generated by the complex turbulent processes in the near-surface layer (e.g., Large and Pond 1982, DeCosmo et al. 1996). The most popular parameterization is to determine bulk coefficients that vary with wind speed and stability (e.g., Friehe and Schmitt 1976; Blanc 1985; Smith 1988; Yelland and Taylor 1996). These formulas depend on more easily measured quantities, such as surface wind speed, surface air temperature, surface specific humidity of the atmosphere, and sea surface temperature, where surface usually means a height on the order of 10 m above the sea surface. The stability is typically accounted for in terms of an air–sea temperature difference and a surface roughness length (e.g., Garratt 1977; Liu et al. 1979). While parameterized bulk formulas are computationally inexpensive, they have difficulty in representing the air–sea fluxes in low wind speed regimes. This is because accounting for buoyancy effects on the turbulent transport becomes especially important, and this evaluation requires using an iteratively recursive stability-dependent algorithm.

The turbulence-based formulations also use bulk formulas but strive to take full account of dynamic stability in the near-surface layer. This is achieved in two ways. One is by more accurately determining the bulk coefficients by iteratively solving for the dynamic stability of the atmosphere (Fairall et al. 1996). The other is by more accurately determining the surface properties by carrying additional prognostic equations to characterize the turbulence (Kantha and Clayson 1994). This makes the turbulence models the most computationally expensive of the above-mentioned three methods and becomes a serious consideration when studying decadal and interdecadal variability with large-scale GCMs of high spatial resolution.

Adequately resolving the physical dynamics of the atmosphere and ocean continually drives the need to have a GCM of higher spatial resolution. Every increase in horizontal and vertical resolution requires decreasing the time step for a GCM simulation using explicit numerical schemes, in order to satisfy the Courant–Friedrichs–Lewy limit for computational stability (Haltiner and Williams 1980). For example, every two-fold increase in horizontal resolution requires a four-fold increase in computer memory and about an eight-fold increase in computer processing time. These computer resource requirements can severely limit the kind of simulations that are performed with the presently available computer architectures. For example, consider the Naval Research Laboratory (NRL) Layered Ocean Model (NLOM) (Hurlburt et al. 1996), which minimizes computational expense by representing the vertical dimension with only a few isopycnal layers. The global-scale NLOM of approximately $\frac{1}{8}$ deg horizontal resolution, using five isopycnal layers and a surface mixed layer, requires arrays of $2048 \times 1152 \times 6$ for the global domain spanning 72°S–65°N. This global NLOM is run with a time step of 12 min and requires 52 min of wall clock time per month of model simulation when running on one of the fastest parallel architectures currently available, a 176-processor Cray T3E-900. To study the atmosphere and ocean at the highest spatial resolution possible, one therefore always searches for ways to make algorithms as computationally efficient as possible, while retaining the important physical processes

that are essential for a correct GCM simulation. That is, one always searches for a way to balance accuracy and computational efficiency. This includes the GCM algorithms implemented for computing the momentum and heat fluxes.

The purpose of this paper is to present a convenient and computationally less expensive formulation for the calculation of wind stress, and latent and sensible heat fluxes in a GCM. This formulation has an accuracy comparable to air–sea fluxes determined using a stability-dependent algorithm, such as that used for the Tropical Ocean Global Atmosphere Coupled Ocean–Atmosphere Response Experiment (TOGA COARE) as described in Fairall et al. (1996). In this paper, the bulk coefficients are expressed in terms of atmospheric wind speed for different air–sea temperature intervals, such that the stability dependence of these coefficients can be replaced with a simple equation. This provides a computationally inexpensive means by which to perform multiyear GCM simulations that include the major effect of atmospheric dynamic stability.

The paper is organized as follows. In section 2 the datasets and methodology used for determining the relations for the bulk coefficients are described. The bulk formulas are given in section 3. To validate the accuracy of the formulation, we compare the air–sea fluxes obtained using a year-long time series of observations from a mooring in the central Arabian Sea against corresponding air–sea fluxes calculated using the TOGA COARE algorithm. Section 4 compares the computational expense of the method presented in this paper, relative to the standard algorithm adopted by TOGA COARE. Conclusions are presented in section 5.

2. Data and approach

In this study we use the tabulated values of exchange coefficients for wind stress and latent heat flux reported by Bunker (1976) and the exchange coefficients for sensible heat flux reported by Isemer and Hasse (1987). The values of these coefficients were determined from measurements made at several different locations in the global ocean, coastal installations, and within laboratories that were averaged over time periods varying from a few minutes to several hours. Using these values for the exchange coefficients, Bunker (1976) estimated climatological wind stress and surface heat fluxes by exploiting the extensive information residing in compiled ship observations. These ship weather reports spanned the years 1941–72 and contained observations from locations covering the ocean from the equator to 80°N. The dataset used by Bunker (1976) has since been updated by Hasse (1993), who improved upon the estimates for the exchange coefficients by using direct and profile measurements obtained over the open sea. The main differences between the two datasets are that Bunker (1976) included stability dependence using Monin–Obukhov similarity theory in determining the exchange coefficients, and that Bunker did not report the exchange coefficients for sensible heat. In both studies the exchange coefficients were used to calculate wind stress, and sensible and latent heat flux values for each individual ship observation, and these values then averaged to derive monthly fields. A third dataset of bulk coefficients (Smith 1988) has also been compiled using Businger–Dyer flux–gradient formulas (Dyer 1974) in an iterative process. This dataset was not used because it is less comprehensive than those of the first two studies.

The coefficients tabulated from the two studies are in general agreement with each other. However, by evaluating and recalculating Bunker heat fluxes based on updated parameterizations and a revised Beaufort wind scale, Large and Pond (1982) and Isemer et al. (1989) report that the value of latent heat flux coefficient (C_L) should be approximately 13% less than that reported in Bunker (1976). This implies a corresponding overestimation of latent and sensible heat exchange, given ideal input data. However, this kind of systematic error exists in many climatological datasets due to the error caused by ship avoidance of high winds (e.g., Lo and McBean 1978; Weare and Strub 1981). We use these two datasets to construct a new dataset of averaged exchange coefficient values that are used to determine parameterized expressions for the exchange coefficients. As outlined further below, the averages are calculated according to whether the wind speed and air–sea temperature difference value of the individual observations used to derive the exchange coefficient value falls into a given class interval.

Given that the wind drag coefficient is dependent on both the wind speed and the air–sea temperature difference, we can construct a linear equation in $(T_s - T_a)$ with coefficients that vary with the wind speed interval [i.e., $C_D = C_{D0}(V_a) + C_{D1}(V_a)(T_s - T_a)$]. Here C_{D0} and C_{D1} are the intercept and slope of the least squares line, respectively. To obtain these coefficients we plotted air–sea temperature differences against the C_D values given in Table 1 by using the midclass value for each air–sea temperature difference category as given in Table 2. As is evident from the least squares fits, the C_D values correlate strongly with the air–sea temperature differences for all but high wind speeds. Compared to the linear least squares solution, a quadratic fit is found to give the best result for both the C_{D0} and C_{D1} values at all wind speed intervals. The best solution is obtained when using V_a as the dependent variable (Fig. 1). The fitted expressions are

$$C_D = C_{D0} + C_{D1}(T_s - T_a), \tag{1}$$

$$C_{D0} = 10^{-3}[0.862 + 0.088\hat{V}_a - 0.00089(\hat{V}_a)^2], \tag{2}$$

$$C_{D1} = 10^{-3}[0.1034 - 0.00678\hat{V}_a + 0.0001147(\hat{V}_a)^2]. \tag{3}$$

Limits are set on the wind speed as $\hat{V}_a = \max[2.5, \min(32.5, V_a)]$ because the drag coefficient is constant

TABLE 1. Drag coefficient values for the wind stress ($C_D \times 10^3$) given at different intervals of wind speed (V_a) and air–sea temperature differences ($T_a - T_s$).

Air–sea temperature difference (in °C)	Atmospheric wind speed (V_a) at 10 m (in m s^{-1})							
	<5	5 to 10	10 to 15	15 to 20	20 to 25	25 to 30	30 to 35	>35
$T_a - T_s \geq 5.0$	0.06	0.77	1.47	1.95	2.26	2.52	2.78	3.00
$5.0 > T_a - T_s \geq 1.0$	0.60	1.30	1.72	2.04	2.30	2.54	2.79	3.00
$1.0 > T_a - T_s \geq 0.2$	0.98	1.43	1.80	2.10	2.35	2.57	2.80	3.00
$0.2 > T_a - T_s \geq -0.2$	1.20	1.54	1.87	2.16	2.40	2.60	2.80	3.00
$-0.2 > T_a - T_s \geq -1.0$	1.32	1.60	1.90	2.22	2.42	2.62	2.80	3.00
$-1.0 > T_a - T_s \geq -5.0$	1.56	1.78	2.00	2.25	2.44	2.63	2.80	3.00
$-5.0 > T_a - T_s$	1.80	1.86	2.10	2.32	2.48	2.64	2.80	3.00

when $V_a > 35$ m s^{-1}. Note that these equations have been derived for a wind speed measured at a reference height of 10 m above the sea surface.

Since our analyses are based on averages of the data combined under different wind speed categories, we choose to test the significance of the correlation coefficients for no correlation and significance using the *t* test and *z* test, respectively. Details on the application of these tests are given in appendix A. Our null hypothesis for the *t* test is that the two variables C_D and $T_s - T_a$ are not correlated. All the calculated *t* values (Table 2) fall outside the acceptance region of $-1.96 < t < 1.96$, and the null hypothesis is therefore rejected. For the *z* test a correlation coefficient (r) of 0.7 is used as the demarcation point for significance. Fisher's *z* transform (Wilks 1995) is applied to test the significance of *r* values.

The stability-dependent latent and sensible heat flux coefficents (C_L and C_S, respectively) reported from both datasets above are provided in Table 3 according to wind speed (V_a) intervals and air–sea temperature differences ($T_a - T_s$). Note that the C_S values are very close to C_L and are smaller. This is not surprising because the sensible heat flux over the ocean is generally small compared to the latent and radiational exchanges. In addition, the errors in the total heat budget that result from the assumption of equal coefficents are found to be negligible (Geernaert et al. 1986; Geernaert 1990). Thus the dependence of C_L on stability is expected to be the same as that of C_S. This assumption is acceptable if humidity is a minor contributor to stratification in the atmosphere. The exception is when dry air is advected over the sea surface, as the stratification is then mainly determined by the evaporation of moisture at the air–sea interface (Greenhut 1982).

The dependences of the latent heat flux coefficients on V_a and $T_a - T_s$ are shown in Fig. 2. This illustration differs slightly from the one shown in Smith (1988) in that we only show the variation of the latent heat flux coefficient with respect to the logarithmic wind speed for the given air–sea temperature difference intervals. At large wind speeds the C_L values converge toward a value of approximately 1.7×10^{-3}. Note that when $T_a > T_s$, the C_L values are smaller than those when $T_a < T_s$.

Similar to the C_D coefficients, we can construct an equation for C_L that has a dependence on both the wind speed and the air–sea temperature difference such that $C_L = C_{L0}(V_a) + C_{L1}(V_a)\,(T_s - T_a)$. Again, C_{L0} and C_{L1} are the intercept and slope of the least squares line, respectively (Fig. 3). The same analysis with similar results (not shown) has also been performed for C_S. The constant and intercept of each linear solution for both C_L and C_S are given in Table 4. Also included are the correlation coefficients (r) between the air–sea temperature difference and C_L (C_S). Note that the C_L (C_S) values correlate strongly with the air–sea temperature differences for all wind speed categories.

Using the slope and intercept values (Table 4) we numerically determine the wind speed dependence values of C_{L0} and C_{L1}. Compared to the linear least squares solution, a quadratic fit is found to be the best for both

TABLE 2. Linear least square fits of wind drag coefficients with respect to sea–air temperature difference ($T_s - T_a$) at each wind speed (V_a) interval. The values for $C_{D0}(V_a)$ and $C_{D1}(V_a)$ are obtained for each wind speed interval, separately. The slope $C_{D0} \times 10^3$, the intercept $C_{D1} \times 10^3$, and correlation coefficients (r) are given for each wind speed interval. The significance of the correlation coefficients are tested using both the *t* value and *z* value as described in appendix A. The standard error is calculated using $1/\sqrt{n-3}$, where $n = 7$ stands for the number of cases. The decision regarding the significance of an *r* value is made relative to a correlation coefficient value of 0.7.

Wind speed	Slope	Intercept	*r* value	*t* value	*z* value	z_{diff}/err.	Significant?
$0 < V_a \leq 5$	0.090	1.07	0.96	7.67	1.95	2.16	Yes
$5 < V_a \leq 10$	0.057	1.47	0.95	6.80	1.83	1.93	No
$10 < V_a \leq 15$	0.033	1.84	0.98	11.01	2.30	2.86	Yes
$15 < V_a \leq 20$	0.020	2.15	0.95	6.80	1.83	1.93	No
$20 < V_a \leq 25$	0.012	2.37	0.94	6.16	1.74	1.74	No
$25 < V_a \leq 30$	0.007	2.59	0.90	4.62	1.47	1.21	No
$30 < V_a \leq 35$	0.001	2.80	0.91	4.91	1.53	1.32	No
$35 < V_a \leq 40$	0.005	1.86	0.98	11.01	2.30	2.86	Yes

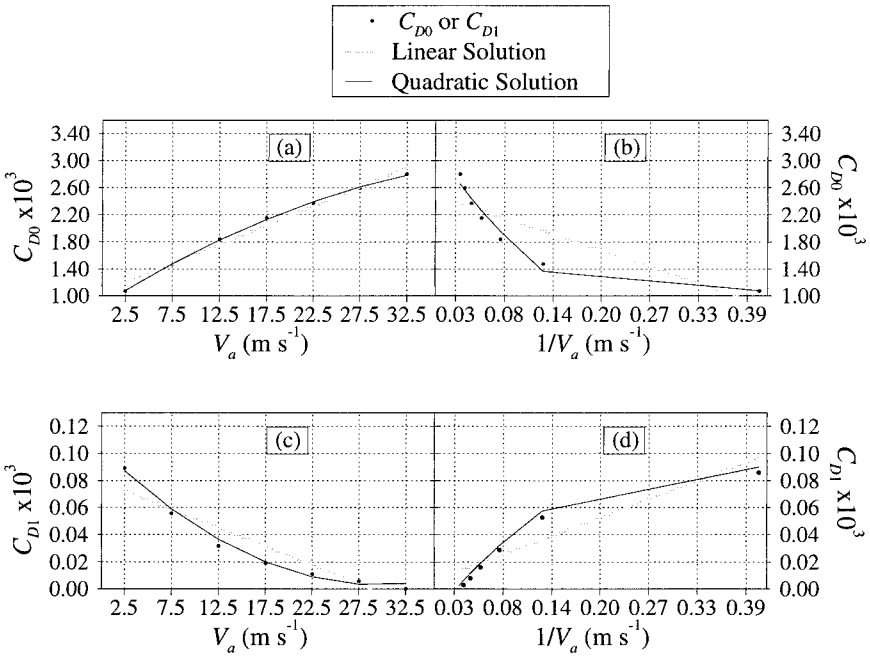

FIG. 1. Linear and quadratic fits to the slope (C_{D0}) and intercept (C_{D1}) values shown in Table 2. Examination is made using both wind speed (V_a) and inverse wind speed ($1/V_a$) as the dependent variables to determine the best fit: (a) C_{D0} vs V_a, (b) C_{D0} vs $1/V_a$, (c) C_{D1} vs V_a, and (d) C_{D1} vs $1/V_a$.

the C_{L0} and C_{L1} values at all wind speed intervals (Fig. 4). The best solution for C_{L0} is obtained when using V_a as the dependent variable, while for C_{L1} the best solution is with $1/V_a$ as the dependent variable. The fitted expressions are as follows:

$$C_L = C_{L0} + C_{L1}(T_s - T_a), \quad (4)$$

$$C_{L0} = 10^{-3}[0.994 + 0.061\hat{V}_a - 0.001(\hat{V}_a)^2] \quad (5)$$

$$C_{L1} = 10^{-3}[-0.020 + 0.691(1/\hat{V}_a) - 0.817(1/\hat{V}_a)^2], \quad (6)$$

where the wind speed is limited to the interval $\hat{V}_a = \max[3.0, \min(27.5, V_a)]$. Limits are imposed on V_a for C_{L0} and C_{L1} [Eqs. (5) and (6)] to suppress the underestimation of the quadratic fit when $V_a > 27.5$ m s^{-1}.

Because the C_L values are so close in value to the C_S (see Table 3), we elect to find a linear relationship between C_L and C_S rather than determine independent C_{S0} and C_{S1} coefficients. This also helps to reduce the cost of computing the sensible heat flux in GCMs. The simplest representative linear formulation is found to be $C_S = 0.96\ C_L$ with a negligible intercept (3.6×10^{-6}).

TABLE 3. The latent heat flux coefficient ($C_L \times 10^3$) as a function of wind speed (V_a) and air–sea temperature difference ($T_a - T_s$) intervals. The values in parentheses are for the sensible heat flux coefficient ($C_S \times 10^3$).

Air–sea temperature difference (in °C)	Atmospheric wind speed (V_a) Interval at 10 m (in m s^{-1})							
	<3	3 to 6	6 to 9	9 to 12	12 to 15	15 to 20	20 to 25	>25
$T_a - T_s \geq 5.0$	0.07	0.22	0.69	1.06	1.39	1.59	1.74	1.81
	(0.07)	(0.21)	(0.66)	(1.01)	(1.33)	(1.52)	(1.66)	(1.73)
$5.0 > T_a - T_s \geq 1.0$	0.30	0.67	1.17	1.36	1.58	1.68	1.79	1.84
	(0.29)	(0.65)	(1.12)	(1.30)	(1.51)	(1.60)	(1.72)	(1.76)
$1.0 > T_a - T_s \geq 0.2$	0.72	1.12	1.36	1.48	1.61	1.75	1.83	1.85
	(0.69)	(1.07)	(1.30)	(1.42)	(1.55)	(1.67)	(1.75)	(1.77)
$0.2 > T_a - T_s \geq -0.2$	1.32	1.34	1.44	1.53	1.64	1.80	1.86	1.86
	(1.27)	(1.28)	(1.38)	(1.46)	(1.57)	(1.72)	(1.78)	(1.78)
$-0.2 > T_a - T_s \geq -1.0$	1.65	1.45	0.46	1.58	1.68	1.82	1.86	1.87
	(1.58)	(1.38)	(1.40)	(1.51)	(1.60)	(1.74)	(1.78)	(1.78)
$-1.0 > T_a - T_s \geq -5.0$	2.05	1.68	1.58	1.65	1.74	1.86	1.86	1.88
	(1.96)	(1.60)	(1.51)	(1.58)	(1.66)	(1.78)	(1.78)	(1.78)
$-5.0 > T_a - T_s$	2.52	2.01	1.79	1.79	1.84	1.94	1.93	1.90
	(2.41)	(1.93)	(1.72)	(1.72)	(1.76)	(1.86)	(1.84)	(1.82)

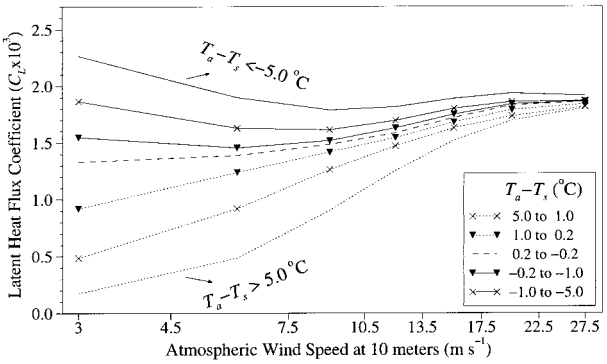

FIG. 2. Variation of latent heat flux coefficient (C_L) with air and sea temperature difference ($T_a - T_s$) for given wind speed intervals. A two-point moving average has been applied to smooth the coefficients. Note the C_L values are on the order of 10^3, and the x axis is logarithmic.

Values from the datasets are found to have a correlation coefficient of $r = 0.99$.

3. Verification of air–sea fluxes

a. Buoy data

For this study we have chosen to use a year-long time series of meteorological observations from a mooring in the central Arabian Sea (Fig. 5) to assess the performance of our methodology. The Arabian Sea can produce some of the highest latent heat fluxes in the global ocean due to strong seasonal winds (e.g., Jourdan and Gautier 1995). This region is well known to have strong surface winds (Latif et al. 1994) that seasonally alternate direction from the northeast during the boreal winter to the southwest during the boreal summer (Fig. 6).

The timing and intensity of the monsoon cycle varies for different regions within the Arabian Sea. In November, the northeast monsoon begins with steady northeast winds that last until February, with the winds being less intense than the southwest monsoon. The latter begins in May with the onset of winds from the southwest, produces the strongest winds in the central Arabian Sea in July in a feature called the Findlater jet (Findlater 1966), and then diminishes rapidly in September with the onset of the fall intermonsoon period. Note here that the spring intermonsoon, from February through May, is characterized by reduced winds and variable directionality. These strong monsoon winds, together with the periods of light winds in the spring and fall, were recorded by a Woods Hole Oceanographic Institution (WHOI) buoy moored near the Findlater jet axis during the 1994–95 cooperative research expedition (Weller et al. 1998). The datasets from this mooring provide a high-frequency meteorological record over a large range

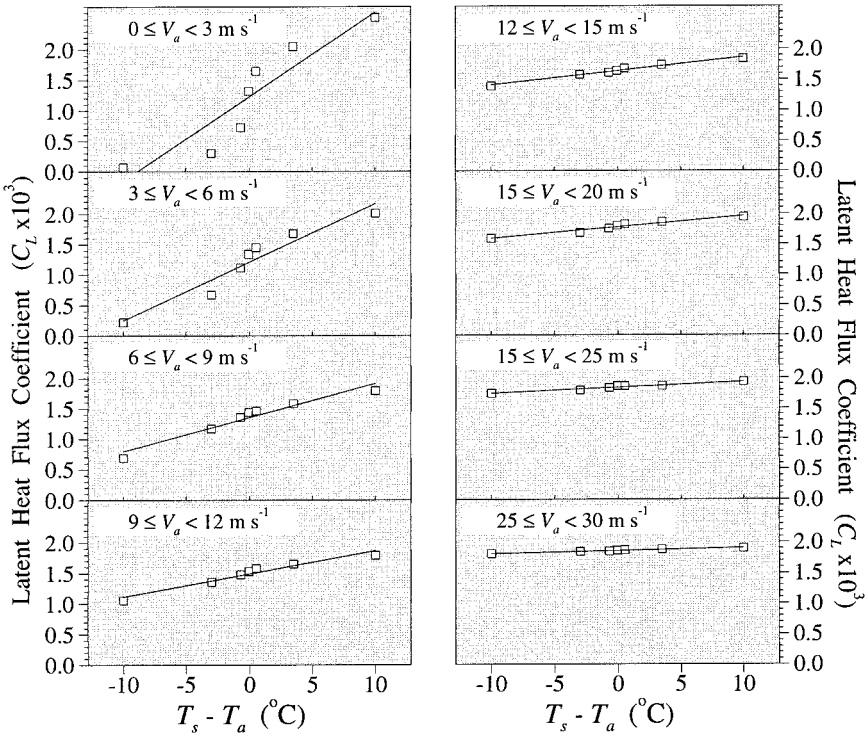

FIG. 3. Variation of latent heat flux coefficient (C_L) with respect to sea–air temperature difference ($T_s - T_a$) for each given wind speed interval. The solid line shows the linear least squares fit whose slope and intercept is used for determining the C_{L0} and C_{L1} values, respectively (see Table 4). The C_L values have been scaled by 10^3.

TABLE 4. Linear least square fits of latent (sensible) heat flux coefficients with respect to sea–air temperature difference ($T_s - T_a$) at each wind speed (V_a) interval. The values for C_{L0} (V_a) and C_{L1} (V_a) are obtained for each wind speed interval, separately. The slope $C_{L0} \times 10^3$ ($C_{S0} \times 10^3$), the intercept $C_{L1} \times 10^3$ ($C_{S1} \times 10^3$), and correlation coefficients (r) are also given for each wind speed interval. The statistical significance of the correlation coefficients are tested using both the t value and z value as described in appendix A. The standard error is calculated using $1/\sqrt{n-3}$, where $n = 7$ stands for the number of cases. The decision regarding the significance of an r value is made in comparison to a 0.7 correlation coefficient. Note that the values in parentheses are for sensible heat flux coefficients.

Wind speed	Slope	Intercept	r value	t value	z value	z_{diff}/err.	Significant?
$0 < V_a \leq 3$	1.227	0.138	0.92	5.25	1.59	1.44	No
	(1.176)	(0.132)	(0.91)	(4.91)	(1.53)	(1.32)	(No)
$3 < V_a \leq 6$	1.209	0.096	0.96	7.67	1.95	2.16	Yes
	(1.156)	(0.092)	(0.97)	(8.92)	(2.09)	(2.45)	(Yes)
$6 < V_a \leq 9$	1.353	0.056	0.97	8.92	2.09	2.45	Yes
	(1.296)	(0.054)	(0.97)	(8.92)	(2.09)	(2.45)	(Yes)
$9 < V_a \leq 12$	1.491	0.037	0.97	8.92)	2.09	2.45	Yes
	(1.427)	(0.036)	(0.98)	(11.01)	(2.30)	(2.86)	(Yes)
$12 < V_a \leq 15$	1.639	0.020	0.99	15.69	2.65	3.56	Yes
	(1.568)	(0.022)	(0.99)	(15.69)	(2.65)	(3.56)	(Yes)
$15 < V_a \leq 20$	1.776	0.019	0.97	8.92	2.09	2.45	Yes
	(1.698)	(0.018)	(0.97)	(8.92)	(2.09)	(2.45)	(Yes)
$20 < V_a \leq 25$	1.838	0.010	0.97	8.92	2.09	2.45	Yes
	(1.758)	(0.009)	(0.97)	(8.92)	(2.09)	(2.45)	(Yes)
$25 < V_a \leq 30$	1.858	0.005	0.98	11.01	2.30	2.86	Yes
	(1.774)	(0.004)	(0.97)	(8.92)	(2.09)	(2.45)	(Yes)

of wind speeds and have been used to compute air–sea fluxes with the TOGA COARE algorithm. The availability of these air–sea fluxes with the meteorological observations makes this an ideal source with which to verify our methodology and assess its accuracy relative to a fully stability-dependent formulation.

The mooring record has a continuous time series of air and sea surface temperatures, air specific humidity, and wind speed/direction data, at a 7.5-min sampling interval or less, spanning from 1 November 1994 to 15 October 1995. A time series of daily averages of these quantities are shown in Fig. 7. Since wind speed is the most common quantity in the bulk formulas used here, we elect to separate our observation period into two monsoon periods [northeast (NE) and southwest (SW)] and two intermonsoon periods (spring and fall). These

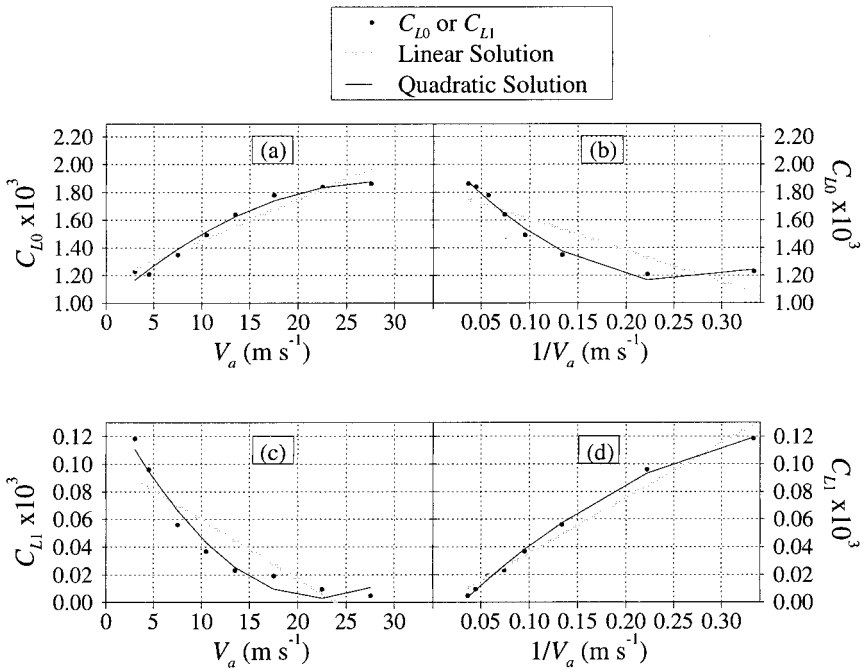

FIG. 4. Linear and quadratic fits to the slope (C_{L0}) and intercept (C_{L1}) values shown in Table 4. Examination is made using both wind speed (V_a) and inverse wind speed ($1/V_a$) as the dependent variables to determine the best fit: (a) C_{L0} vs V_a, (b) C_{L0} vs $1/V_a$, (c) C_{L1} vs V_a, and (d) C_{L1} vs $1/V_a$.

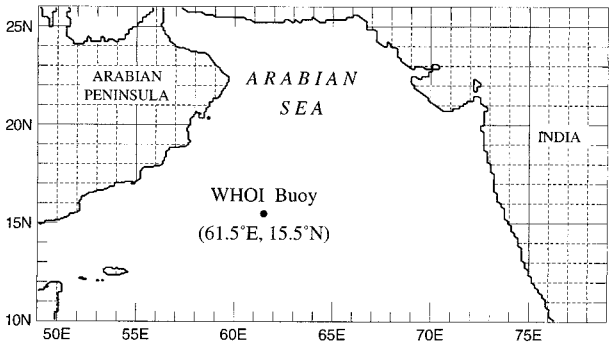

FIG. 5. The location of the WHOI mooring deployed during the 1994–95 Arabian Sea Experiment. During its deployment the mooring measured the surface meteorological parameters at a sampling rate of 7.5 min and higher. Further details regarding measurements can be found in Weller et al. (1998). The land–sea boundary shown in gray shade is the 200-m isobath.

time periods are defined to be consistent with Weller et al. (1998).

The NE monsoon in 1994 was characterized by steady but moderate winds, while the SE monsoon was characterized by strong winds and moist air having large mixing ratio values (see Fig. 7). Note that the wind speed is much larger ($\approx$10 m s^{-1}) during the SW monsoon compared to the other periods. Air temperatures are usually colder than sea surface temperatures during the boreal winter when the NE monsoon is active, and the air and sea specific humidity differences remain approximately constant at around 6 g kg^{-1}. In contrast, when the SW monsoon is active, air temperatures are higher than sea surface temperatures, thereby making air–sea temperature differences positive. During this period, the average of the differences in air–sea mixing ratio (2.9 g kg^{-1}) is relatively small in comparison to the air–sea mixing ratio differences during the NE monsoon (Table 5).

In this study we use daily averages of air–sea fluxes computed using the TOGA COARE algorithm as our reference (observed) fluxes. The TOGA COARE algorithm is designed to give estimates of the wind stress and air–sea fluxes using stability-dependent exchange coefficients of heat and momentum (Fairall et al. 1994, 1996). This algorithm employs a turbulence theory based on the classic Monin–Obukhov similarity approach along with very detailed parameterizations. These include the effects of rainfall (Gosnell et al. 1995) and wind gusts (Godfrey and Beljaars 1991), representing surface transfer processes in terms of roughness parameters, and using dimensionless profile functions that asymptotically approach the proper convective limit when the wind speed goes to zero.

b. Wind stress

The wind stresses for the buoy are those from Weller et al. (1998) and were calculated using the TOGA COARE algorithm as described therein. The wind

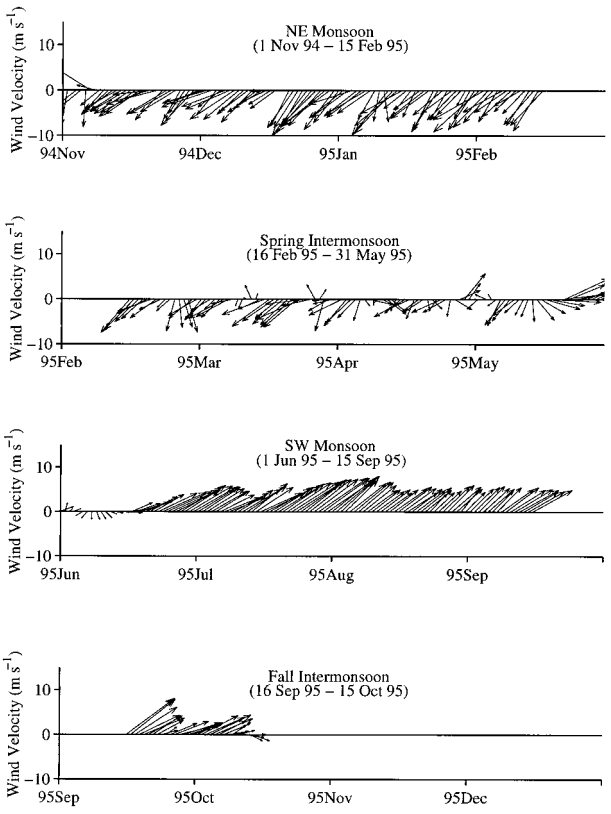

FIG. 6. Wind direction and magnitude for the monsoon and intermonsoon periods (1 Nov 1994–15 Oct 1995) examined in this study. The wind vectors are shown every day during the period. The length of an arrow corresponds to the magnitude of the wind speed. Note that northeasterly and southwesterly winds are dominant during the NE and SW monsoon periods.

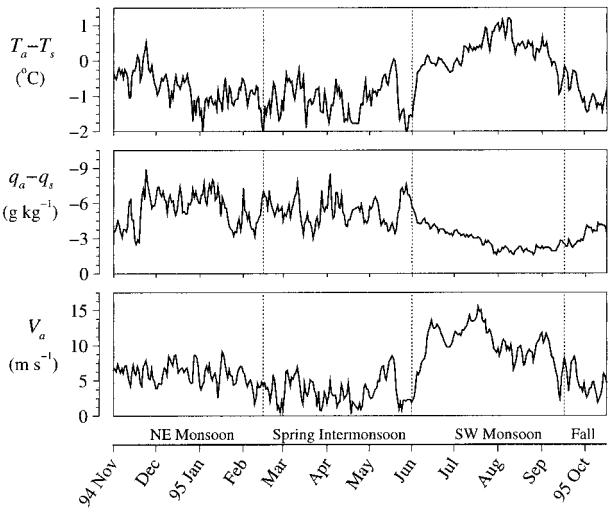

FIG. 7. Time series of air–sea temperature differences ($T_a - T_s$), air–sea mixing ratio differences ($q_a - q_s$), and 10-m atmospheric wind speed by the buoy. The observations are shown for the time period used in this study (1 Nov 1994–15 Oct 1995). For the location of the buoy see Fig. 5.

TABLE 5. Mean values of air–sea temperature difference ($\overline{T_{\text{diff.}}} = \overline{T_a - T_s}$, air–sea humidity difference ($\overline{q_a - q_s}$), and wind speed ($\overline{V_a}$) for the 1994–95 monsoon periods. The values are obtained from the 24-h averages of the data time series. Start and end dates of each monsoon period are also given, along with the number of days (N).

Monsoon type	Time period		N	$\overline{T_{\text{diff}}}$	$\overline{q_a - q_s}$	$\overline{V_a}$
	Start date	End date	(day)	(°C)	(g kg^{-1})	(m s^{-1})
NE monsoon	1 Nov 1994	15 Feb 1995	106	−0.8	−5.5	5.9
Spring intermonsoon	16 Feb 1995	31 May 1995	105	−1.1	−5.4	3.6
SW monsoon	1 Jun 1995	15 Sep 1995	108	0.2	−2.9	10.1
Fall intermonsoon	16 Sep 1995	15 Oct 1995	31	−0.9	−3.3	4.8
All period	1 Nov 1994	15 Oct 1995	350	−0.8	−4.3	6.1

stresses [$\boldsymbol{\tau} = (\tau_x, \tau_y)$] computed with our methodology are determined from the wind velocity [$\mathbf{V}_a = (u, v)$] using the nonlinear drag coefficient (C_D) derived in section 2. The time series of $T_a - T_s$ and V_a shown in Fig. 7 are used to determine the daily averaged wind stresses for the comparisons reported here. The wind stress components and magnitude are calculated as follows:

$$\tau_x = \rho_a C_D u(u^2 + v^2)^{1/2}, \quad (7)$$

$$\tau_y = \rho_a C_D v(u^2 + v^2)^{1/2}, \quad (8)$$

$$\tau = \rho_a C_D(u^2 + v^2). \quad (9)$$

Here density of the air (ρ_a) at the air–sea interface is calculated using the ideal gas law formulation ($\rho_a = 100\, P_a/[R_{\text{gas}}(T_a + 273.16)]$ in kg m^{-3}). Figure 8 shows the magnitudes of the wind stresses obtained from the TOGA COARE algorithm and our simpler bulk formulas.

Note here that the buoy data provide a wide variation in wind conditions with which to test the accuracy of our method for determining the wind stress. The SW monsoon is characterized by strong winds with an average speed of approximately 10 m s^{-1}, while the NE monsoon is characterized by steady but moderate winds with an average speed of approximately 6 m s^{-1}. During the intermonsoon periods light wind conditions of 0–5 m s^{-1} prevailed. Over this entire range of conditions (i.e., 1 November 1994 to 15 October 1995) the TOGA COARE algorithm and our method are found to yield wind stresses that are in quite good agreement with each other (Fig. 9), having bias[1] values of 0.0003 and −0.0009 N m^{-2} for τ_x and τ_y, respectively. The correlation coefficients [normalized rmse values (nrmse)] for τ_x and τ_y obtained from the two methodologies are 0.99 (0.22), and 0.99 (0.23), respectively. Note here that the skill scores are very high, being very close to 1, with values of 0.71 and 0.83 for τ_x and τ_y, respectively. This agreement is quite remarkable given the large variation in wind speed from the peak values during the NE and SW monsoons (11.0 and 18.4 m s^{-1}, respectively) to the light wind conditions of the intermonsoon periods. For a more detailed discussion of the atmospheric forcing as recorded by the mooring and its impact on upper-ocean properties, the reader is referred to Weller et al. (1998) and Rochford et al. (2000), respectively.

We also estimated the wind stress transferred to the ocean surface by rainfall. Following Caldwell and Elliott (1971) a numerical estimate of the momentum of

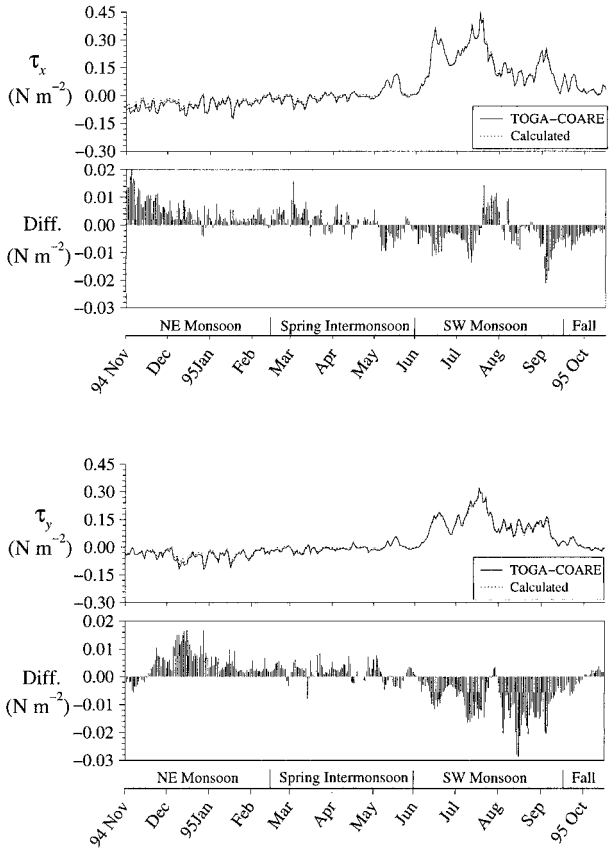

FIG. 8. Time series of the zonal wind stress (τ_x) and merdional wind stress (τ_y) obtained from the stability-dependent TOGA COARE algorithm vs our methodology for 1 Nov 1994–15 Oct 1995. Differences between the two methodologies (calculated-TOGA COARE) during the entire period are shown with impulses, separately.

[1] In this study we use various statistical parameters such as bias, linear correlation coefficient (r), root-mean-square error (rmse), and skill score (SS) to measure the strength of the statistical relationship between our estimated and reference (TOGA COARE) values (e.g., Murphy 1988; Laurent et al. 1998). All these statistical parameters are given in appendix A along with a brief explanation.

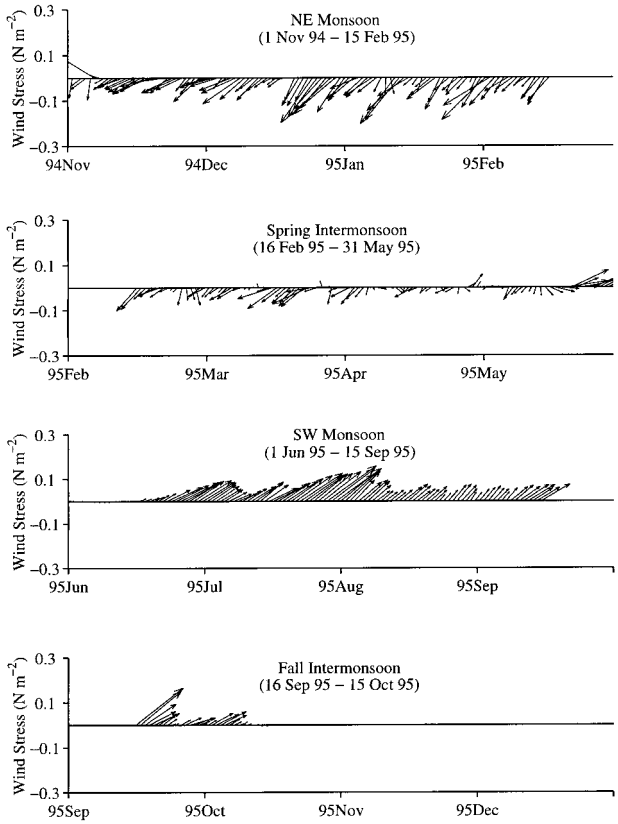

FIG. 9. Wind stress direction and magnitude for the monsoon and intermonsoon periods (1 Nov 1994–15 Oct 1995) examined in this study. The length of an arrow corresponds to the magnitude of the wind speed. The strong wind stress of the NE and SW monsoon periods is evident relative to the intermonsoon periods.

rainfall can be expressed as $\tau_r = RV_a/3600$, where R is the rain rate in millimeters per hour and the water density is implicit. This calculation yielded wind stress values from 0 to 0.006 N m^{-2}. Overall, the ratio of wind stress to wind stress due to rainfall (i.e., τ/τ_r) was only 0.009 during the observation period. Since this 0.9% effect is very small, the contribution due to rainfall was neglected in our calculations.

c. Sensible and latent heat flux estimates

The sensible and latent heat fluxes for the buoy are those given in Weller et al. (1998). Our daily averaged latent and sensible heat fluxes are determined using the expressions for latent and sensible heat flux coefficients (C_L and C_S, respectively) given in section 2. We use the time series of meteorological variables ($T_a - T_s$, $q_a - q_s$, and V_a) shown in Fig. 7 with the following bulk aerodynamic equations for latent ($L \times E$) and sensible (H) heat flux:

$$H = C_S C_p \rho_a V_a (T_a - T_s), \tag{10}$$

$$L \times E = C_L L \rho_a V_a (q_a - q_s), \tag{11}$$

$$\rho_a = \frac{100 P_a}{[R_{\text{gas}}(T_a + 273.16)]}, \tag{12}$$

$$q_a = \text{RH}\, q_{\text{sat}}(T_a), \tag{13}$$

$$q_{\text{sat}}(T) = \frac{0.622 e_s(T)}{P_a - 0.378 e_s(T)}, \tag{14}$$

$$q_s = 0.98 q_{\text{sat}}(T_s), \tag{15}$$

$$e_s(T) = (1 + 3.46 \times 10^{-6} P_a) 6.1121 \times \exp[17.50T/(240.97 + T)]. \tag{16}$$

The parameters appearing in Eqs. (10)–(16) are defined in appendix B along with their units. Similar to wind stresses presented in section 3b, the density of the air is calculated using the gas law. Note the mixing ratio values for air (q_a at T_a) and sea (q_s at T_s) are calculated using a simplified version of the original formulation for saturated vapor pressure (e_s) presented by Buck (1981). Similar to the air and sea mixing ratio, e_s is also calculated at T_a and T_s for air and sea, respectively. Because we derived the wind drag, and sensible and latent heat flux coefficients using global data, the atmospheric pressure (P_a) at the sea surface is treated as constant and equal to the standard atmospheric pressure (i.e., 1013 mb). The average air pressure for the buoy observation period used here was 1010.5 mb.

Although it would be more accurate to estimate the latent heat flux at the air–sea interface using the ocean skin temperature (Fairall et al. 1996), we have elected instead to use T_s in our formulation. It has been shown that using T_s in the bulk scheme, and thereby neglecting the effects of the warm layer or cool skin, usually yields reasonable estimates of the fluxes on climate timescales (Zhang 1995). Given that GCMs are typically applied for basin-scale climate studies, the neglect of the small temperature differences produced by warm layer and cool skin effects is not a significant constraint. During heavy precipitation events, the contribution of cold rain to the sensible heat flux can be very large (Webster 1994). However, during the obervation period for the buoy used here there was not a significant amount of rainfall. Thus, we ignored the contribution of precipitation in determining the sensible heat flux.

There is clearly a good agreement between the reference values and our estimates for both the latent and sensible heat fluxes (Fig. 10), with small bias values of 16.1 and -0.9 W m^{-2}, respectively. Note that in the TOGA COARE algorithm q_s is expressed as 0.98 times the saturation mixing ratio of pure water at the sea surface, because reduction in water vapor pressure by salinity in the sea water had to be taken into account in the equatorial regions. In our calculation of q_s this factor is also taken into account for consistency because our

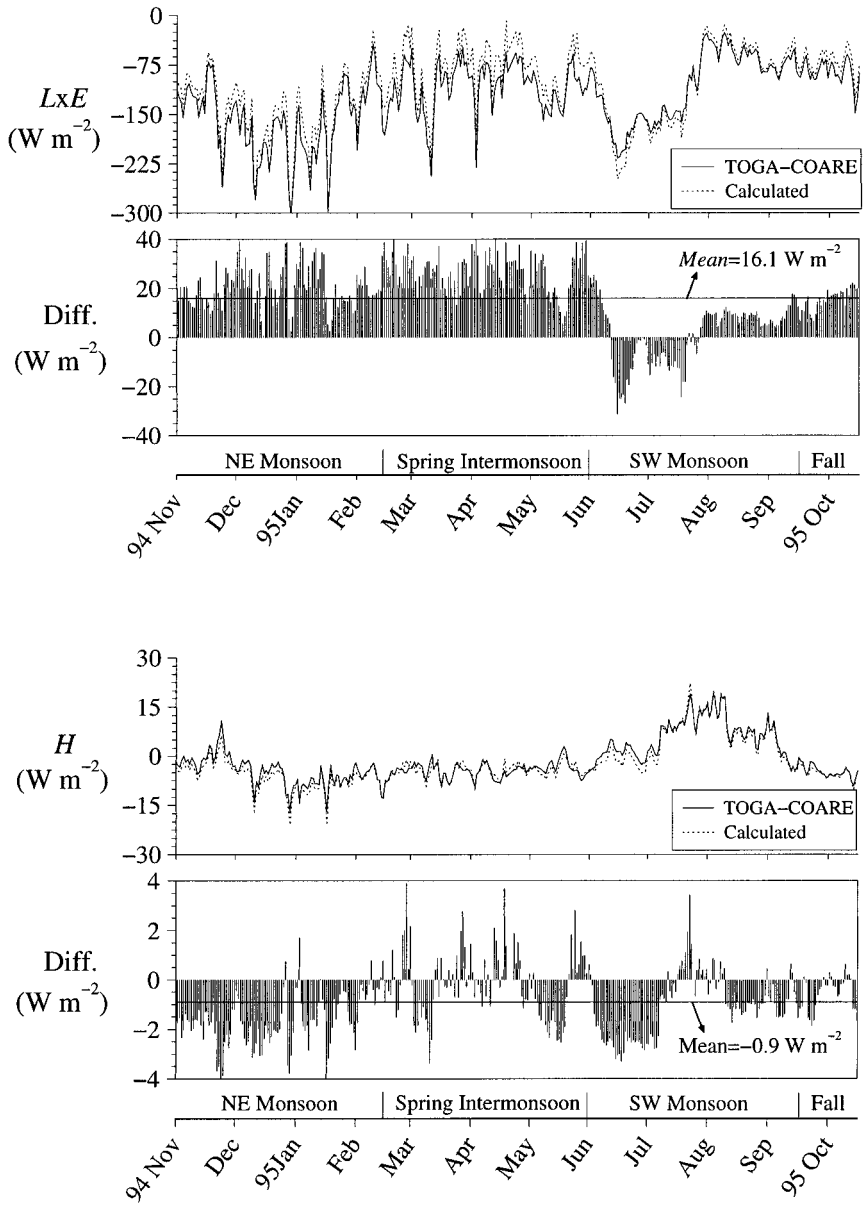

FIG. 10. Time series of latent heat fluxes ($L \times E$) and sensible (H) heat fluxes obtained from the stability-dependent TOGA COARE algorithm vs our methodology from 1 Nov 1994 to 15 Oct 1995. The differences between the two methodologies (calculated-TOGA COARE) are shown with impulses, separately, along with mean error (me) during the whole period.

buoy location is close to the equator. A scatterplot (Fig. 11) shows that our methodology tends to overestimate the latent heat fluxes in comparison to the reference values. Approximately 87% (306 out of 350 cases) of our calculated latent heat flux estimates are larger than the reference fluxes. However, the reverse is true for the sensible heat fluxes, with our sensible heat fluxes tending to slightly underestimate relative to the reference values. Approximately 25% (85 out of 350 cases) of our calculated sensible heat fluxes are larger than the reference fluxes.

Even though there are strong winds, the latent heat flux during the SW monsoon is not very large overall because $q_a - q_s$ is relatively small during this period (see Fig. 7). The latent heat flux during the NE monsoon is much large in contrast, even though the winds are much weaker. The winds during the NE monsoon advect cold air southward over the relatively warm ocean surface to form an unstable atmospheric boundary layer. This unstable vertical stratification may enhance downward transport of momentum fluxes, which increases the wind speed near the surface and thereby generates

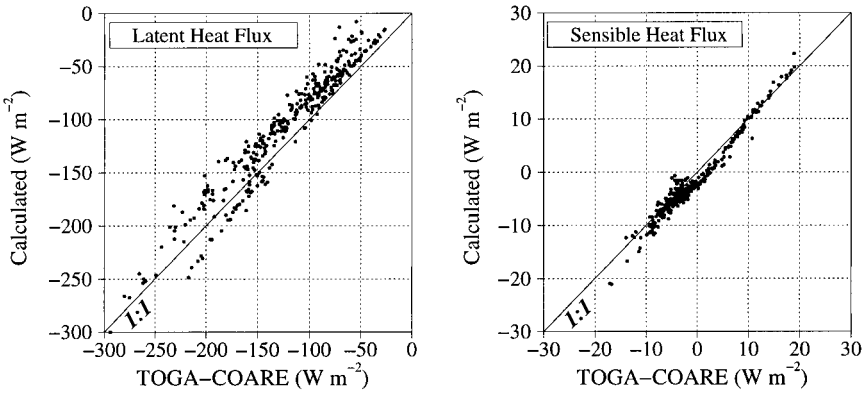

FIG. 11. Scatterplots of latent ($L \times E$) and sensible (H) heat fluxes obtained from the stability-dependent TOGA COARE algorithm vs our methodology from 1 Nov 1994 to 15 Oct 1995. The correlation coefficients (r) are 0.97 and 0.98 for the latent and sensible heat fluxes between the two datasets, respectively. Note the number of cases (n) is 350 for the entire time period, 1 Nov 1995–15 Oct 1995. For a detailed statistical evaluation see also Table 6.

a substantial increase in the latent heat fluxes. For a very simple stability condition, the $T_a - T_s$ values indicate relatively unstable conditions near the bottom of the atmospheric boundary layer. These unstable conditions appear to occur at the WHOI mooring site whenever the wind speed is less than $\approx$10 m s^{-1} (Fig. 7).

The skill scores greater than 0.3 calculated for all monsoon and intermonsoon periods indicate that we are obtaining reasonable agreement between our estimates and the reference fluxes (Table 6). Note that the best SS value for the latent heat flux occurs for the NE monsoon, while the best SS for the sensible heat flux occurs for the SW monsoon. The nrmse values show the errors for our estimates vary from 15% to 33% (20%–41%) of the TOGA COARE values for the latent (sensible) heat fluxes. Considering the square of r values given in Table 6, one finds almost 100% of the variance in the TOGA COARE latent heat fluxes is reproduced by our estimates. During the fall intermonsoon, the SS is relatively small because the latent heat fluxes are close to each other, and the standard deviation of the reference fluxes is only 19 W m^{-2}, while it is 54, 38, and 23 W m^{-2} for the NE monsoon, spring intermonsoon, and SW monsoon, respectively. Examination of the slopes of the least squares line (see appendix A) indicates all slope values are close to 1 for the monsoon and intermonsoon periods, and serves as another indication of the good estimates provided by our calculated fluxes.

TABLE 6. Statistical verification of the latent ($L \times E$) and sensible heat fluxes (H) between reference TOGA COARE values and our methodology. Comparisons are made for the monsoon and intermonsoon periods. A detailed description regarding the statistical parameters is provided in appendix A.

Heat flux	N (day)	r	me (W m^{-2})	rmse (W m^{-2})	nrmse	SS	a
NE monsoon							
Latent	106	0.98	20.4	22.7	0.16	0.81	1.00
Sensible	106	0.94	−1.7	2.0	0.24	0.80	0.94
Spring intermonsoon							
Latent	105	0.97	25.4	29.6	0.33	0.43	1.00
Sensible	105	0.82	−0.1	1.4	0.42	0.65	0.77
SW monsoon							
Latent	108	0.99	1.0	12.2	0.15	0.72	1.20
Sensible	108	0.99	−1.0	1.6	0.30	0.93	1.15
Fall intermonsoon							
Latent	31	0.97	15.0	15.7	0.19	0.32	0.95
Sensible	31	0.94	−0.6	0.9	0.35	0.78	0.83
All period							
Latent	350	0.97	16.1	20.5	0.22	0.86	1.03
Sensible	350	0.98	−0.9	1.6	0.20	0.94	1.01

As a final verification, we compare the latent and sensible heat fluxes obtained with the two methodologies for the wind speed intervals used in deriving the fitted expressions for C_L and C_S. The purpose is to determine if a systematic bias has been introduced in arriving at these fitted expressions, and to what extent it has (if any) on the accuracy of our bulk formulas. Comparison of our calculated latent and sensible heat fluxes relative to the reference fluxes (Fig. 12) indicates good agreement, especially for wind speeds greater than 3 m s^{-1}. Note here that limits are imposed on V_a in Eqs. (5) and (6) to suppress the underestimation of the desired fit at low and very high wind speeds. The most interesting feature of Fig. 12 is that our calculated latent heat flux is usually overestimated for any given wind speed interval, while the sensible heat fluxes for the same interval are usually underestimated. This is due to $T_a - T_s$ usually being positive when V_a is relatively large (e.g., during SW monsoon), thereby making the sensible heat flux differences positive. In general, the relatively large SS values and small nrmse, mean error (me) and rmse for both latent and sensible heat flux estimates (Fig. 13) show our methodology yields very close results in comparison to a stability-dependent formulation

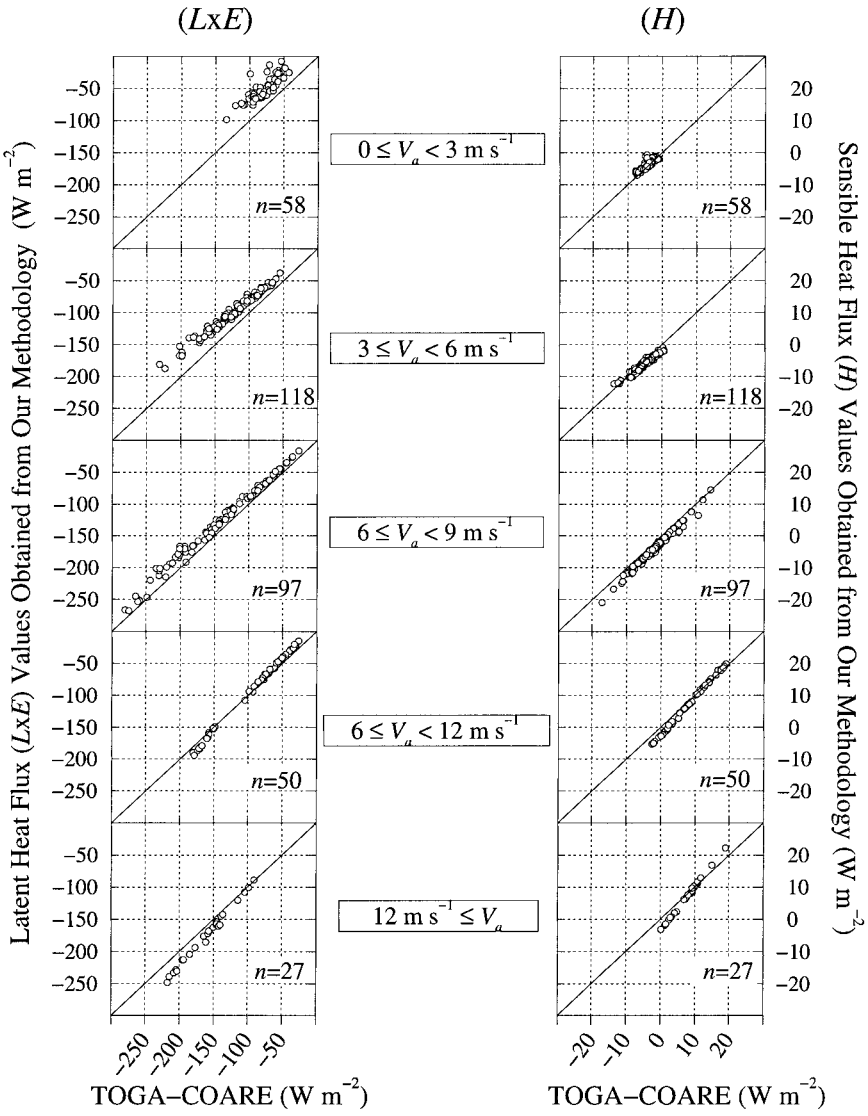

FIG. 12. Estimation of the latent ($L \times E$) and sensible (H) heat fluxes obtained from our methodology vs the latent and sensible heat fluxes from the reference TOGA COARE dataset for 1 Nov 1994–15 Oct 1995. The analysis is shown at different wind speed intervals, and the number of cases (n) is also given for each category.

for all wind speed invervals. The SS is lowest for the light wind interval (0–3 m s^{-1}) because our methodology does not include the effects of wind gustiness as in the TOGA COARE algorithm. The neglect of this and other physical processes included in the TOGA COARE algorithm is the reason for the small differences in the air–sea fluxes between the two methods. Clearly, the neglect of such processes does not appreciably diminish the accuracy of our method and will not significantly influence GCM predictions on timescales of a week or longer.

We finally note here that the standard bulk coefficients may be used with an uncertainty of 5% or less when considering climatological sensible and latent heat flux values. However, much larger uncertainties can occur for time-averaged fluxes of a day or less. This is due to the short averaging period for the winds producing a 5%–10% uncertainty in the root-mean-square error (Marsden and Pond 1983).

4. Computational expense of method

To properly simulate dynamics at mesoscales in the atmosphere and eddy-resolving scales in the ocean, GCMs need to be run at high horizontal resolution and short time steps. For an AGCM, this is typically 1°–3° horizontal resolution and hundreds of seconds time resolution [e.g., 1.5° and 1200 s for the Navy Operational

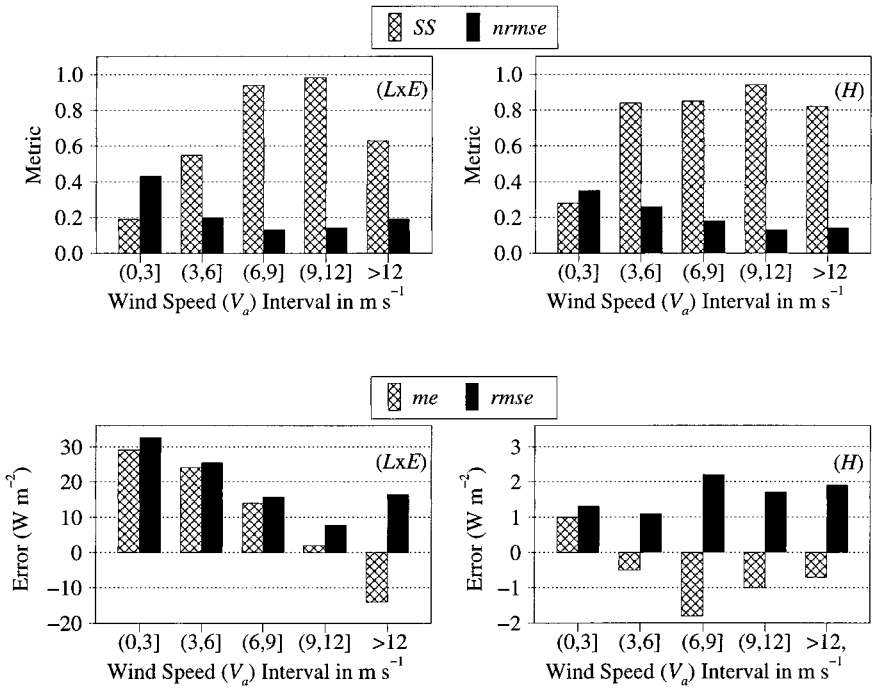

FIG. 13. Skill score (SS), nrmse, me, and rmse values for the latent ($L \times E$) and sensible (H) heat fluxes obtained from our methodology vs the reference TOGA COARE values. The statistics are shown for ($L \times E$) and H at given atmospheric wind speed (V_a) intervals, separately. On the x axis labels, (0, 3] denotes $0 \leq V_a < 3$, etc. Note that the SS and nrmse are unitless.

Global Atmospheric Prediction System (Hogan and Rosmond 1991)]. For an OGCM, this is less than 1° horizontal resolution and tens of minutes [e.g., ⅛ deg and 12 min for NLOM (Hurlburt et al. 1996)]. These requirements translate into an enormous number of calculations when performing high-resolution global AGCM and OGCM simulations over one annual cycle. For example, for the above NLOM case, six arrays of 2048×1152 must be time evolved 120 time steps for a 1-day simulation of a single physical variable. This is on the order of 1.7×10^9 computations and represents a minimum estimate, as it ignores the computation of the individual terms in the prognostic equations. The actual computational cost when expressed in computer processing unit (cpu) time is ≈9 cpu hours per month of model simulation when running on a 176-processor Cray T3E-900, or 3.1 cpu min per processor. This cost becomes very expensive when performing climate studies on decadal to interdecadal timescales, and it is prohibitive for simulations using high-resolution coupled GCMs. With future GCMs expected to be of even higher spatial resolution, there will be only further increased demands on computer resources.

Any measures that can improve the efficiency of a GCM, while sufficiently preserving the accuracy of its simulation, merit serious consideration. This includes the GCM algorithms for air–sea fluxes. As shown here, the simple bulk formulas introduced in this paper have an accuracy comparable to that of the more complex TOGA COARE algorithm and are therefore quite suitable for use in a GCM. Their simplicity implies they are computationally inexpensive and would increase GCM efficiency. To obtain an indication of the computational savings, we measured the cpu time required to calculate the wind stress and air–sea fluxes with these formulas and the TOGA COARE algorithm. These measurements were made on a Sun Ultra 1 Model 140 computer workstation with 320 MB of main memory. The wind stress and air–sea fluxes from both methods were calculated within the publicly available FORTRAN 77 (F77) program that is distributed as the COARE Met Flux Algorithm. The cpu time for execution of the F77 program segment containing each method was determined using the DTIME Sun system library function. Two datasets were used for the benchmarks. One was the daily averaged buoy time series containing 366 records, and the other was the time series of 116 records provided as test data for the COARE Met Flux Algorithm.

The calculation of wind stress and heat fluxes for both datasets required less than 0.5 cpu seconds for each of the methods. While the TOGA COARE algorithm is fast for such one-dimensional time series, the bulk formulas are 27.3 and 28.7 times faster for the buoy and test datasets, respectively. The greater amount of cpu time required by the TOGA COARE algorithm is pro-

portional to the 20 iterations required by the latter for its atmospheric surface layer calculations of roughness and stability. The bulk formulas are clearly much less computationally expensive and are a preferred choice for use in any high-resolution GCM. Benchmark simulations using the bulk formulas and TOGA COARE algorithm in a GCM was not performed because of the computational costs. Preference is to save valuable computer resources for GCM simulations exploring physical processes rather than spend them on studies of computational efficiency.

5. Conclusions

Through a statistical analysis of drag, and latent and sensible heat flux coefficients derived from surface meteorological observations, we have introduced here simple bulk formulas for air–sea fluxes that are computationally inexpensive to use in GCMs. These formulas account for dynamic stability in the atmosphere via a simple polynomial dependence on wind speed and a linear dependence on the air–sea temperature difference. They are applicable for use with 10-m wind speeds and provide an accuracy comparable to more robust methods such as the TOGA COARE algorithm. The latter determines the turbulent air–sea fluxes through a recursive solution for the atmospheric dynamic stability and is taken here as the best method presently available.

Using mooring data from the central Arabian Sea, we have shown these bulk formulas provide air–sea fluxes that agree with TOGA COARE to a high level of accuracy over the wide range of wind speeds prevalent for this ocean basin. Differences in the results between our methodology and the stability-dependent TOGA COARE algorithm are very small and on the order of $\pm 1 \times 10^{-3}$ N m^{-2} for wind stress, ± 15 W m^{-2} for latent heat flux, and ± 1 W m^{-2} for sensible heat flux. This accuracy is sufficient for most GCM applications of interest. The simplicity of these bulk formulas makes them computationally less expensive to use than more complex algorithms. Simple test comparisons found them to be approximately 30 times faster than the standard algorithm adopted by TOGA COARE. This accuracy and ease of computation make these bulk formulas a preferred method for computing air–sea fluxes in computationally expensive GCMs. Our experience in using these formulas in the global NLOM with an embedded mixed layer has already proven them to be computationally inexpensive. Future versions of this model will be more highly resolved in space and time and will benefit from a more efficient air–sea flux algorithm.

Acknowledgments. The dataset for the Arabian Sea buoy was provided courtesy of Robert A. Weller at the Woods Hole Oceanographic Institution (WHOI), Woods Hole, Massachussetts. The COARE-Met Flux Algorithm was provided courtesy of the Center for Ocean–Atmosphere Prediction Studies (COAPS), The Florida State University, Tallahassee, Florida, with special thanks to David M. Legler. Discussions with Alan J. Wallcraft and John C. Kindle at NRL during the preparation of this manuscript are warmly acknowledged. Additional thanks go to Chris W. Fairall of Environmental Technology Laboratory of NOAA for his helpful discussions regarding the flux calculations. This work was funded by the Office of Naval Research (ONR) and is a contribution of the Basin-Scale Prediction System project under Program Element 602435N and the Dynamics of Coupled Models Project under Program Element 61153N. Sverdrup Technology, Inc., is funded under subcontract from NRL. This is Contribution NRL/JA/7323-99-0033 and has been approved for public release.

APPENDIX A

Statististical Definitions

Let v_i ($i = 1, 2, \ldots, n$) be the set of n reference values (i.e., heat fluxes from TOGA COARE), and let e_i ($i = 1, 2, \ldots, n$) be the set of estimates (i.e., heat fluxes from our methodology). Also let v (e) and σ_v (σ_e) be the mean and standard deviations of the reference (estimate) values, respectively. Given these definitions, the statistical relationships between our estimated latent (sensible) heat fluxes and the ones obtained from the reference TOGA COARE algorithm can be expressed as given below.

The mean error (i.e., bias) is the difference between the mean estimate e and the mean reference value v,

$$\text{me} = \overline{e} - \overline{v}. \tag{A1}$$

The linear correlation coefficient (r) measures the cofluctuation between the estimate and reference, and it is not sensitive to a bias. In our analyses, an r value greater than 0.7 is considered a good correlation.

$$r = \frac{1}{n}\sum_{i=1}^{n} (v_i - \overline{v})(e_i - \overline{e})/(\sigma_v \sigma_e) \tag{A2}$$

To decide if the sample values of r represent a good or poor linear relationship we apply two tests: a) the Student's t-test, and b) Fischer's z transform.

1) *Student's t-test:* This is applied to test the null hypothesis that two variables (e.g., $T_s - T_a$ and C_D) are not correlated for a given wind speed interval. For the $n = 7$ sample of random values in this work, the bivariate normal distribution of $t_{n-2} = r\sqrt{n-2}/\sqrt{1-r^2}$ (e.g., Neter et al. 1988) must have an absolute value of at least 0.66 for r to be statistically significant at the 95% ($\alpha = 0.05$) confidence level. We compare the t value with $t_{0.05}$, and if $t < t_{0.05}$ we accept the null hypothesis that there is no linear relationship between the two variables. The null hypothesis can be rejected for t values that fall outside the acceptance region of $-1.96 < t < 1.96$.

2) *Fischer's z transform:* The z test (e.g., Wilks 1995) is used to determine the statistical significance of r in comparison to a correlation coefficient of 0.7. The z value is described as $z = 0.5 \ln[(1 + r) - (1 - r)]$. The null hypothesis is tested if the correlation between the two variables is $r \geq 0.7$ for a given wind speed interval at the 95% ($\alpha = 0.05$) significance level. If $z > z_{0.05}$ we accept the null hypothesis that the correlation is not significant from 0.7. The value of z for $r = 0.7$ (i.e., $|z_{0.7}|$) is 0.87, and that of z for our calculated value $r = 0.92$ (i.e., $|z_r|$) is 1.59, giving a difference ($|z_r - z_{0.7}|$) of 0.72. Since the standard error is 0.5, the difference of our true r value from 0.7 is 1.44 (=0.72/0.5). At the $\alpha = 0.05$ significance level the range is ± 1.96, so a 0.92-correlation efficient is not significant from 0.7.

The root-mean-square error (rmse) can be considered as an absolute measure of the distance between the estimate and reference values:

$$\text{rmse}^2 = \frac{1}{n} \sum_{i=1}^{n} (e_i - v_i)^2. \tag{A3}$$

The nondimensional skill score (SS) is sensitive to bias. It is equal to 1 for a perfect estimate ($e_i = v_i$) and is equal to 0 for the best constant estimate ($e_i = \overline{v}$). This nondimensional skill score (Murphy 1988) can be interpreted as a relative measure of the distance between the estimate and reference:

$$\text{SS} = 1 - \frac{\text{rmse}^2}{\sigma_v^2}. \tag{A4}$$

The normalized root-mean-square error (nrmse) is also a measure of the relative distance between the estimate and reference. The scaling factors have different meanings for SS and nrmse. The SS depends on the standard deviation of the reference data set, while nrmse depends on the corresponding mean as given below. Note that for small values of v_i the contribution to nrmse would be very large:

$$\text{nrmse}^2 = \frac{1}{n} \sum_{i=1}^{n} \left[\frac{(e_i - v_i)}{v_i} \right]^2. \tag{A5}$$

The slope a of the linear regression (i.e., $v = ae + b$) is used for determining under-/overestimation of the calculated values (amplitude bias) with respect to a reference value. The importance of examining the coefficient a of the linear regression in the validation procedure is discussed in Morissey and Janowiak (1996):

$$a = r \frac{\sigma_e}{\sigma_v}. \tag{A6}$$

APPENDIX B

List of Symbols

a	Slope of linear regression line
C_D	Wind stress drag coefficient
C_L	Latent heat flux coefficient
C_S	Sensible heat flux coefficient
C_p	Specific heat of air (1004.5 J kg^{-1} K^{-1})
e_s	Saturated water vapor pressure at T_s (mb)
$\overline{e}$	Mean of estimated air–sea flux values (W m^{-2})
H	Sensible heat flux (W m^{-2})
L	Latent heat of vaporization (2.5×10^6 J kg^{-1})
$L \times E$	Latent heat flux (W m^{-2})
me	Mean error (W m^{-2})
n	Number of cases in the statistical analysis
N	Number of days in a monsoon or intermonsoon period
nrmse	Normalized root-mean-square error
P_a	Atmospheric pressure at sea surface (1013 mb)
q_a	Air mixing ratio at 10 m above sea level (g kg^{-1})
q_s	Saturation mixing ratio at temperature T (g kg^{-1})
r	Linear correlation coefficient
R	Rain rate (mm h^{-1})
R_{gas}	Gas constant (287.1 J kg^{-1} K^{-1})
RH	Relative humidity (%)
rmse	Root-mean-square error (W m^{-2})
SS	Skill score
T_a	Air temperature at 10 m above sea level (°C)
T_s	Sea surface temperature (°C)
u	Zonal wind speed component (m s^{-1})
v	Meridional wind speed component (m s^{-1})
V_a	Wind speed at 10 m above sea level (m s^{-1})
ρ_a	Air density at the air–sea interface (kg m^{-3})
σ_e	Standard deviation of estimated values (W m^{-2})
σ_v	Standard deviation of reference (observed) values (W m^{-2})
τ	Wind stress ($\tau_x^2 + \tau_y^2$)$^{1/2}$ magnitude (N m^{-2})
τ_r	Wind stress due to rainfall (N m^{-2})
τ_x	Zonal component of wind stress (N m^{-2})
τ_y	Meridional component of wind stress (N m^{-2})
$\overline{v}$	Mean of reference (observed) flux values (W m^{-2})

REFERENCES

Atlas, R., 1987: The role of oceanic fluxes and initial data in the numerical prediction of an intense coastal storm. *Dyn. Atmos. Oceans,* **10,** 359–388.

——, A. J. Busalacchi, M. Ghil, S. Bloom, and E. Kalnay, 1987: Global surface wind and flux fields from model assimilation of Seasat data. *J. Geophys. Res.,* **92,** 6477–6487.

Barnier, B., 1998: Forcing the ocean. *Ocean Modeling and Parameterization,* E. P. Chassignet and J. Verron, Eds., Kluwer, 45–80.

Blanc, T. V., 1985: Variation of bulk-derived surface flux, stability, and roughness results due to the use of different transfer coefficient schemes. *J. Phys. Oceanogr.,* **15,** 650–669.

Buck, A. L., 1981: New equations for computing vapor pressure and enhancement factor. *J. Appl. Meteor.,* **20,** 1527–1532.

Bunker, A. F., 1976: Computations of surface energy flux and annual air–sea interaction cycles of the North Atlantic Ocean. *Mon. Wea. Rev.,* **104,** 1122–1140.

Caldwell, D. R., and W. P. Elliott, 1971: Surface stresses produced by rainfall. *J. Phys. Oceanogr.,* **1,** 145–148.

Chen, D., A. J. Busalacchi, and L. M. Rothstein, 1994: The roles of vertical mixing, solar radiation, and wind stress in a model sim-

ulation of the sea surface temperature seasonal cycle in the tropical Pacific Ocean. *J. Geophys. Res.*, **99,** 20 345–20 359.
Chu, P. C., Y. Chen, and S. Lu, 1998: On Haney-type surface boundary conditions for ocean circulation models. *J. Phys. Oceanogr.*, **28,** 890–901.
Cummings, J. A., C. Szczechowski, and M. R. Carnes, 1997: Global and regional ocean thermal analysis systems. *Mar. Technol. Soc. J.*, **31,** 63–75.
da Silva, A. M., C. C. Young, and S. Levitus, 1994: *Algorithms and Procedures.* Vol. 1, *Atlas of Surface Marine Data 1994, NOAA Atlas NESDIS*, 83 pp.
DeCosmo, J., K. B. Katsaros, S. D. Smith, R. J. Anderson, W. A. Oast, K. Bumke, and H. Chadwick, 1996: Air–sea exchange of water vapor and sensible heat: The Humidity Exchange Over the Sea (HEXOS) results. *J. Geophys. Res.*, **101,** 12 001–12 016.
Dyer, A. J., 1974: A review of flux–profile relationships. *Bound.-Layer Meteor.*, **7,** 363–372.
Fairall, C. W., J. Kepert, and G. J. Holland, 1994: The effect of sea spray on surface energy transports over the ocean. *Global Atmos. Ocean Syst.*, **2,** 121–142.
——, E. F. Bradley, D. P. Rogers, J. B. Edson, and G. S. Young, 1996: Bulk parameterization of air–sea fluxes for Tropical Ocean-Global Atmosphere Coupled-Ocean Atmosphere Response Experiment. *J. Geophys. Res.*, **101,** 3747–3764.
Findlater, J., 1966: Cross-equatorial jet stream at low level over Kenya. *Meteor. Mag.*, **95,** 353–364.
Friehe, C. A., and K. B. Schmitt, 1976: Parameterization of air–sea interface fluxes of sensible heat and moisture by the bulk aerodynamic formulas. *J. Phys. Oceanogr.*, **6,** 801–809.
Garratt, J. R., 1977: Review of drag coefficients over oceans and continents. *Mon. Wea. Rev.*, **105,** 915–929.
Geernaert, G. L., 1990: Bulk parameterizations for the wind stress and heat fluxes. *Surface Waves and Fluxes*, G. L. Geernaert and W. J. Plant, Eds., Kluwer, 91–172.
——, K. B. Katsaros, and K. Richter, 1986: Variation of the drag coefficient and its dependence on sea state. *J. Geophys. Res.*, **91,** 7667–7679.
Godfrey, J. S., and A. C. M. Beljaars, 1991: On the turbulent fluxes of buoyancy, heat, and moisture at the air–sea interface at low wind speeds. *J. Geophys. Res.*, **96,** 22 043–22 048.
Gosnell, R., C. W. Fairall, and P. J. Webster, 1995: The sensible heat of rainfall in the tropical ocean. *J. Geophys. Res.*, **100,** 18 437–18 442.
Greenhut, G. K., 1982: Stability dependence of fluxes and bulk transfer coefficients in a tropical boundary layer. *Bound.-Layer Meteor.*, **24,** 253–264.
Haltiner, G. J., and R. T. Williams, 1980: *Numerical Prediction and Dynamic Meteorology.* 2d ed. John Wiley and Sons, 477 pp.
Hasse, L., 1993: Observations of air sea fluxes. *Energy and Water Cycles in the Climate System*, E. Raschke and D. Jacop, Eds., Springer-Verlag, 263–293.
Hogan, T. F., and T. E. Rosmond, 1991: The description of the navy operational global atmospheric prediction system's spectral forecast model. *Mon. Wea. Rev.*, **119,** 1786–1815.
Hurlburt, H. E., A. J. Wallcraft, W. Schmitz Jr., P. J. Hogan, and E. J. Metzger, 1996: Dynamics of the Kuroshio/Oyashio current system using eddy-resolving models of the North Pacific Ocean. *J. Geophys. Res.*, **101,** 941–976.
Isemer, H. J., and L. Hasse, 1987: *The Bunker Climate Atlas of the North Atlantic Ocean.* Vol. 2. Springer-Verlag, 252 pp.
——, J. Willebrand, and L. Hasse, 1989: Fine adjustment of large scale air–sea energy flux parameterizations by direct estimates of ocean heat transport. *J. Climate*, **2,** 1173–1184.
Jourdan, D., and C. Gautier, 1995: Comparison between global latent heat flux computed from multisensor (SSM/I and AVHRR) and from in situ data. *J. Atmos. Oceanic Technol.*, **12,** 46–72.
Kallberg, P., 1998: Aspects of the re-analysed climate. ECMWF Re-Analysis Project Report Series, Vol. 2, European Centre for Medium-Range Weather Forecasts, 89 pp.
Kantha, L. H., and C. A. Clayson, 1994: An improved mixed layer model for geophysical applications. *J. Geophys. Res.*, **99,** 25 235–25 266.
Kara, A. B., J. B. Elsner, and P. H. Ruscher, 1998: Numerical models of boundary layer processes over and around the Gulf of Mexico during a return-flow event. *Wea. Forecasting*, **13,** 921–933.
Large, W. G., and S. Pond, 1982: Sensible and latent heat flux measurements over the ocean. *J. Phys. Oceanogr.*, **12,** 464–482.
Latif, M., A. Sterl, M. Assenbaum, M. M. Junge, and E. Maier-Reimer, 1994: Climate variability in a coupled GCM. Part II: The Indian Ocean and monsoon. *J. Climate*, **7,** 1449–1462.
Laurent, H., I. Jobart, and A. Toma, 1998: Validation of satellite and ground-based estimates of precipitation over the Sahel. *Atmos. Res.*, **47–48,** 651–670.
Liu, W. T., K. B. Katsaros, and J. A. Businger, 1979: Bulk parameterization of air–sea exchanges of heat and water vapor including the molecular constraints at the interface. *J. Atmos. Sci.*, **36,** 1722–1735.
Lo, A. K., and G. A. McBean, 1978: On the relative errors in methods of flux calculations. *J. Appl. Meteor.*, **17,** 1704–1711.
Marsden, R. F., and S. Pond, 1983: Synoptic estimates of air–sea fluxes. *J. Mar. Res.*, **41,** 349–373.
McCreary, J. P., P. K. Kundu, and R. L. Molinari, 1993: A numerical investigation of dynamics, thermodynamics and mixed layer processes in the Indian Ocean. *Progress in Oceanography*, Vol. 31, Pergamon, 181–244.
Morissey, M. K., and J. E. Janowiak, 1996: Sampling-induced conditional biases in satellite climate-scale rainfall estimates. *J. Appl. Meteor.*, **35,** 541–548.
Murphy, A. H., 1988: Skill scores based on the mean square error and their relationships to the correlation coefficient. *Mon. Wea. Rev.*, **116,** 2417–2424.
Murtugudde, R., R. Seager, and A. Busalacchi, 1996: Simulation of the tropical oceans with an ocean GCM coupled to an atmospheric mixed-layer model. *J. Climate*, **9,** 1795–1815.
Neter, J., W. Wasserman, and G. A. Whitmore, 1988: *Applied Statistics.* Allyn and Bacon, 1006 pp.
Price, J. F., R. A. Weller, C. M. Bowers, and M. G. Briscoe, 1987: Diurnal response of sea surface temperature observed at the Long-Term Upper Ocean Study (34°N, 70°W) in the Sargasso Sea. *J. Geophys. Res.*, **92,** 14 480–14 490.
Roberts, C. M., C. Gordon, and C. Cooper, 1997: The origin of flux adjustments in a coupled model. *Mon. Wea. Rev.*, **125,** 909–925.
Rochford, P. A., J. C. Kindle, P. C. Gallacher, and R. A. Weller, 2000: Sensitivity of the Arabian Sea mixed layer to 1994–1995 operational wind products. *J. Geophys. Res.*, **105,** 14 141–14 162.
Sausen, R., K. Barthel, and K. Hasselmann, 1988: Coupled ocean–atmosphere models with flux adjustment. *Climate Dyn.*, **2,** 145–163.
Shriver, J. F., and H. E. Hurlburt, 1997: The contribution of the global thermohaline circulation to the Pacific to Indian Ocean throughflow via Indonesia. *J. Geophys. Res.*, **102,** 5491–5511.
Smith, S. D., 1988: Coefficients for sea surface wind stress, heat flux and wind profiles as a function of wind speed and temperature. *J. Geophys. Res.*, **93,** 15 467–15 472.
Stull, R. B., 1988: *An Introduction to Boundary Layer Meteorology.* Kluwer, 666 pp.
Swenson, M. S., and D. V. Hansen, 1999: Tropical Pacific Ocean mixed layer heat budget: The Pacific cold tongue. *J. Phys. Oceanogr.*, **29,** 69–81.
Weare, B. C., and P. T. Strub, 1981: The significance of sampling biases on calculated monthly mean oceanic surface heat flux. *Tellus*, **33,** 211–224.
Webster, P. J., 1994: The role of hydrological processes in ocean–atmosphere interactions. *Rev. Geophys.*, **34,** 427–476.
Weller, R. A., M. F. Baumgartner, S. A. Josey, A. S. Fischer, and J. C. Kindle, 1998: Atmospheric forcing in the Arabian Sea during

1994–1995: Observations and comparisons with climatology models. *Deep-Sea Res.,* **45,** 1961–1999.

Wilks, D. S., 1995: *Statistical Methods in the Atmospheric Sciences.* Academic Press, 467 pp.

Yelland, M. J., and P. K. Taylor, 1996: Wind stress measurements from the open ocean. *J. Phys. Oceanogr.,* **26,** 541–558.

Yuen, C. W., J. Y. Cherniawsky, C. A. Lin, and L. A. Mysak, 1992: An upper ocean general circulation model for climate studies: Global simulation with seasonal cycle. *Climate Dyn.,* **7,** 1–18.

Zhang, G. J., 1995: Use of monthly mean data to compute surface turbulent fluxes in the tropical Pacific. *J. Climate,* **8,** 3084–3090.